Progress In Electromagnetics Research, Vol. 157, 79–91, 2016

Retro-Directive Beamforming versus Retro-Reflective Beamforming with Applications in Wireless Power Transmission

Xin Wang[1], Bodong Ruan[1], and Mingyu Lu[2, *]

Abstract—This paper studies the difference between retro-directive beamforming technique and retro-reflective beamforming technique in the context of wireless power transmission applications. In all of our studies, a wireless power receiver broadcasts continuous-wave pilot signal; the wireless power transmitter receives and analyzes the pilot signal; finally, the wireless power transmitter transmits continuous-wave power with phase profile conjugate to that of the received pilot signal. Our study demonstrates that a linear equi-spaced antenna array configuration employed by the wireless power transmitter behaves as a retro-directive beamformer when the wireless power receiver resides in the far-zone of the wireless power transmitter, whereas it behaves as a retro-reflective beamformer when the wireless power receiver is not in the far-zone. This paper further investigates two types of array configurations other than linear equi-spaced array when the wireless power transmitter behaves as a retro-reflective beamformer. One is a V-shaped array, which is obtained by deforming the linear equi-spaced array to a "V" shape. The other is termed "perturbed array:" on the basis of linear equi-spaced array, all the elements' locations are perturbed randomly. It is particularly interesting to compare the equi-spaced array and perturbed array. When the wireless power receiver resides 5 or 6 wavelengths away, a 6-element equi-spaced array and a 6-element perturbed array produce the same power level at the near-zone focal point, but the maximum far-zone gain associated with the perturbed array is 1 dB lower than the equi-spaced array. All the conclusions drawn in this paper are supported by numerical results as well as experimental results.

1. INTRODUCTION

Retro-directive beamforming technique has been investigated for decades with the aim of accomplishing efficient wireless power transmission over long distance. Its best-known application is space solar power, in which solar power is scavenged by satellites in the outer space and then transmitted to the earth using microwave beam [1]. When retro-directive beamforming is applied to space solar power, ground station on the earth sends pilot signal to the satellite and the satellite adjusts its power beam's direction to be opposite to the pilot signal's incoming direction. Because space solar power involves a large number of economic and societal issues in addition to technical issues, its feasibility is still under discussion at present. In recent years, research efforts on wireless power transmission are strongly motivated by the practical demand to charge mobile/portable electronic devices (such as wireless sensors) wirelessly. As a distinctive difference from space solar power applications, mobile/portable devices do not require the wireless power transmitter to reside far away, typically closer than 10 meters [2]. In scenarios that call for wireless power transmission over several meters, it is sometimes impossible to identify one explicit direction to characterize the interaction between wireless power transmitter and wireless power receiver.

Received 17 July 2016, Accepted 11 September 2016, Scheduled 3 November 2016

* Corresponding author: Mingyu Lu (mingyu.lu@mail.wvu.edu).

[1] College of Electronic and Information Engineering, Nanjing University of Aeronautics and Astronautics, Nanjing, Jiangsu 211106, China. [2] Department of Electrical and Computer Engineering, West Virginia University Institute of Technology, Montgomery, West Virginia 25136, USA.

Consequently, retro-directive beamforming cannot be directly applied and it is more appropriate to employ retro-reflective beamforming [3]. Retro-reflective beamforming and retro-directive beamforming share the same fundamental principle, which is using pilot signal to guide power propagation. Whereas the wireless power transmitter in retro-directive beamforming behaves as a conventional phased array antenna, the wireless power transmitter in retro-reflective beamforming is more like a near-field focusing antenna. In other words, the wireless power transmitter in retro-reflective beamforming is desired to construct a focal point at the wireless power receiver's location, which resides in the transmitter's near-zone (rather than far-zone). To be more important, the wireless power transmitter in retro-reflective beamforming is not desired to construct any focal points other than the wireless power receiver's location and its far-zone gain must be minimized to prevent electromagnetic interference. Relative to retro-directive beamforming, far less research has been devoted to retro-reflective beamforming. Particularly, "focusing in near-zone without high gain in far-zone," as the primary characteristic of retro-reflective beamforming, has not been investigated comprehensively.

As a matter of fact, "focusing in near-zone without high gain in far-zone" has various applications in addition to wireless power transmission, such as microwave-induced hyperthermia, microwave remote sensing, RFID, and three-dimensional spatial division multiplexing [4]. Arecibo reflector antennas [5] and quasi-optical lens antennas [6] were demonstrated capable of focusing fields as optical lens. In recent years, planar reflectors [7] and planar lens [8] were designed to focus near-fields. Leaky-wave lens is another type of well-studied configuration to achieve near-field focusing [9–11]. Many researchers take advantage of planar antenna array (composed of microstrip elements, for instance) to achieve focusing in the near-zone [12–20]. Compared to the above methods, retro-reflective beamforming technique focuses electromagnetic fields with the aid of pilot signal such that the focal point coincides with the location from which the pilot signal is broadcasted, thus is more suitable for wireless power transmission applications [3, 21, 22].

This paper aims to study the difference between retro-directive beamforming technique and retro-reflective beamforming technique in the context of wireless power transmission applications. Because retro-reflective beamforming is not as well-investigated as retro-directive beamforming, this paper focuses on the characteristic of "focusing in near-zone without high gain in far-zone" associated with retro-reflective beamforming. In all of our studies, a wireless power receiver broadcasts continuous-wave pilot signal, the wireless power transmitter receives and analyzes the pilot signal, and finally the wireless power transmitter transmits continuous-wave power with phase profile conjugate to the pilot signals' phase profile. Our study starts with linear equi-spaced array configuration for the wireless power transmitter. When the wireless power receiver is in the far-zone of the wireless power transmitter, the equi-spaced array behaves as a retro-directive beamformer; in other words, the equi-spaced array generates a power beam toward the wireless power receiver and a large far-zone gain is resulted. When the wireless power receiver is not in the far-zone of the equi-spaced array, the equi-spaced array approaches a retro-reflective beamformer: the maximum far-zone gain drops while a near-zone focal point is generated at the wireless power receiver's location. Our study further shows that far-zone gain could be reduced by adjusting the array's geometrical configuration without affecting focusing in the near-zone. Specifically, two types of array configurations other than linear equi-spaced array are investigated. One is a V-shaped array, which is obtained by deforming the linear equi-spaced array to a "V" shape. The other one is termed a "perturbed array:" on the basis of linear equi-spaced array, all the elements' locations are perturbed randomly. It is particularly interesting to compare the equi-spaced array and perturbed array. When the wireless power receiver resides 5 or 6 wavelengths away, a 6-element equi-spaced array and a 6-element perturbed array produce the same power level at the near-zone focal point, but the maximum far-zone gain associated with the perturbed array is 1 dB lower than the equi-spaced array. All the conclusions drawn in this paper are supported by numerical results as well as experimental results.

The rest of this paper is organized as follows. Theoretical studies on retro-directive beamforming and retro-reflective beamforming are conducted in Section 2. Section 3 presents some experimental results to verify the theoretical studies of Section 2. And finally, Section 4 relates to our conclusions.

2. THEORETICAL STUDIES OF RETRO-DIRECTIVE BEAMFORMING AND RETRO-REFLECTIVE BEAMFORMING

The underlying principle of conventional retro-directive beamforming technique is illustrated in Figure 1 in the context of wireless power transmission applications. A wireless power transmitter is assumed to be composed of a linear array of equi-spaced antenna elements. A wireless power receiver is assumed to reside in the far-zone of the wireless power transmitter. The operation of retro-directive beamforming technique consists of two steps. In the first step, the wireless power receiver broadcasts pilot signal (which is assumed to be a continuous-wave of low power level). Since the wireless power receiver resides in the far-zone of wireless power transmitter, pilot signal reaches the wireless power transmitter as a plane wave with planar equi-phase surfaces, as depicted in Figure 1(a). As a result, the phases detected by the array's elements exhibit a linear pattern. In the second step, the wireless power transmitter transmits wireless power (which is assumed to be a continuous-wave with the same frequency as pilot signal's but of high power level) to the wireless power receiver. Each antenna element is excited with phase negative to the phase of pilot signal received in the first step, as shown in Figure 1(b); in other words, the phase profile of wireless power transmission in the second step is conjugate to the phase profile of pilot signal reception in the first step. According to the theory of phased array, the wireless power transmitter generates a plane wave with propagation direction opposite to the pilot signal's incoming direction. Retro-directive beamforming technique assures that wireless power propagation is guided toward the location from which the pilot signal is originated, thus is considered an excellent candidate to accomplish wireless power transmission over long distance (on the order of meters or even kilometers, such as in space solar power applications) [23].

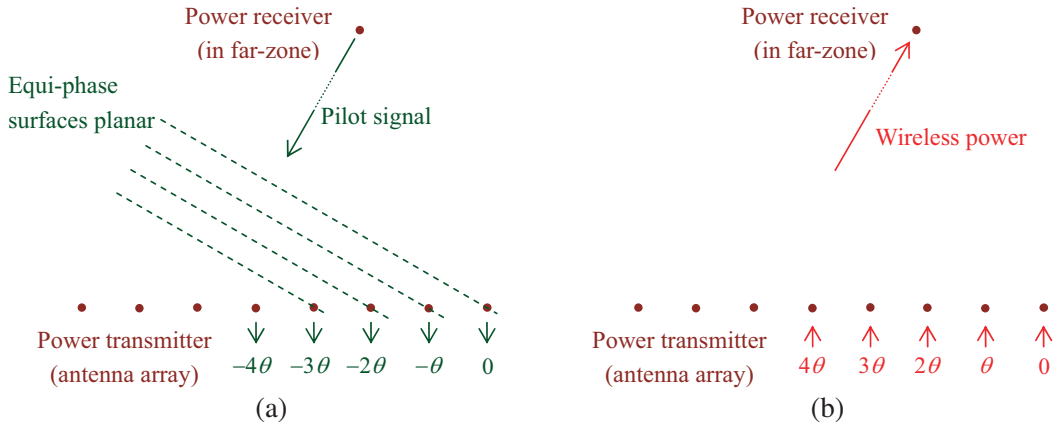

Figure 1. Illustration of retro-directive beamforming technique for wireless power transmission. (a) Wireless power receiver broadcasts pilot signal to wireless power transmitter. (b) Wireless power transmitter sends power to wireless power receiver.

If the wireless power receiver does not reside in the far-zone of wireless power transmitter, the scenario in Figure 1 evolves to Figure 2. In the first step, the pilot signal no longer behaves as a plane wave when it reaches the wireless power transmitter; rather, its equi-phase surfaces are curved, as illustrated by Figure 2(a). Consequently, the phase profile of pilot signal received by the antenna elements does not exhibit linear pattern. When the phase received by the right-most element is defined to be zero, the phase received by an element in the middle is denoted as $-\theta$; apparently, phase $-\theta$ corresponds to the extra path marked by a piece of thick line segment in Figure 2(a). If the right-most element is excited with phase zero and the middle element is excited with phase θ in the second step (Figure 2(b)), their radiations reach the wireless power receiver with the same phase, in other words, their radiations are constructive at the wireless power receiver. The above analysis holds true for any elements of the array. Therefore, exciting the array elements with phase profile conjugate to the pilot signal's phase profile leads to focusing wireless power onto the wireless power receiver's location, which is

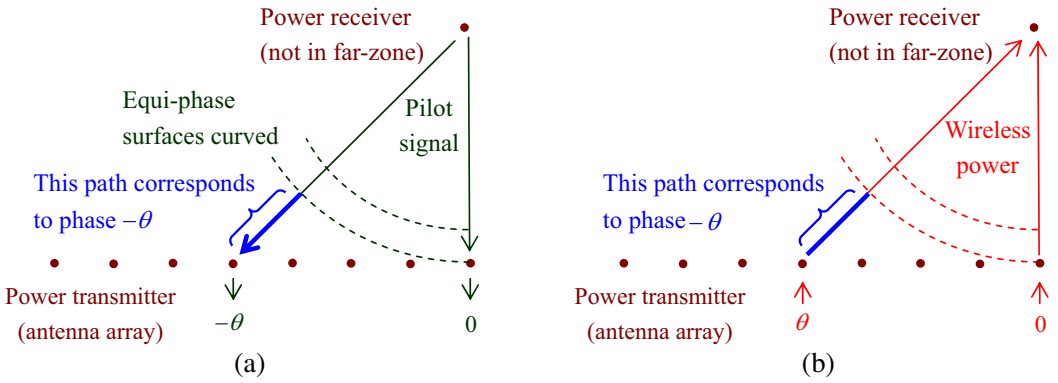

Figure 2. Illustration of retro-reflective beamforming technique for wireless power transmission. (a) Wireless power receiver broadcasts pilot signal to wireless power transmitter. (b) Wireless power transmitter sends power to wireless power receiver.

highly desirable in numerous applications such as charging mobile/portable electronic devices wirelessly. Since neither pilot signal nor wireless power can be characterized by one explicit propagation direction in Figure 2, the scheme illustrated in Figure 2 is retro-reflective beamforming rather than retro-directive beamforming. As a matter of fact, retro-directive beamforming can be considered as a special case of retro-reflective beamforming when the wireless power receiver resides in the far-zone of wireless power transmitter.

The difference between retro-directive beamforming and retro-reflective beamforming is demonstrated by two numerical examples in Figure 3 and Figure 4 respectively.

In the numerical example shown in Figure 3(a), the wireless power transmitter includes six antenna elements. Each element is a Hertzian dipole oriented along z direction. The six-element array is deployed along x axis. The distance between two adjacent elements is $\lambda/2$, with λ denoting the wavelength in free space. The wireless power receiver includes one z-oriented Hertzian dipole, located 40λ away from the spatial origin along $\phi = 70^\circ$ direction. There is only free space other than the wireless power transmitter and wireless power receiver in the entire space, and the electromagnetic fields radiated by Hertzian dipoles in free space are available analytically. In the first step, the wireless power receiver broadcasts pilot signal, a continuous-wave at frequency f, where $f = c/\lambda$ and c is the speed of light in free space. The six elements of the wireless power transmitter detect the pilot signal's phases, denoted as $-\theta_1, -\theta_2, \ldots, -\theta_6$. In the second step, the six elements radiate a continuous-wave at frequency f with uniform amplitude and with phases $\theta_1, \theta_2, \ldots, \theta_6$ respectively. The electric field distribution in a certain region in the x-y plane generated by the six-element array is plotted in Figure 3(b). Because electric field's attenuation follows $1/r$ (with r denoting the distance to the spatial origin) in the far-zone, $|rE_z|^2$ is plotted in Figure 3(b) in order to visualize electric field's far-zone behavior clearly. The $|rE_z|^2$ values in Figure 3(b) are normalized by the largest $|rE_z|^2$ in region $x \in [-\lambda, 10\lambda]$ and $y \in [\lambda, 10\lambda]$. Since the wireless power receiver resides in the far-zone of wireless power transmitter, the six-element array behaves as a retro-directive beamformer. As expected, a directive beam along $\phi = 70^\circ$ is launched in Figure 3(b), and the $|rE_z|^2$ value increases when the distance toward spatial origin increases along $\phi = 70^\circ$. This observation is confirmed by Figure 3(c), in which the far-zone gain values of the six-element array are plotted; specifically, the gain value toward $\phi = 70^\circ$ is as large as 10.15 dBi.

The numerical example in Figure 4 has only one difference from the numerical example in Figure 3: the wireless power receiver is located 5λ away from the spatial origin along $\phi = 70^\circ$ direction. Figure 4(b) shows that $|rE_z|^2$ reaches the largest value at location ($x = 1.7\lambda$, $y = 4.7\lambda$), i.e., electric field is focused onto the wireless power receiver's location. Meanwhile at locations far away from the origin along $\phi = 70^\circ$ direction, the field in Figure 4(b) is not as convergent as that in Figure 3(b). It is also observed from Figure 4(c) that the gain value along $\phi = 70^\circ$ is 9.6 dBi, 0.55 dB lower than the 10.15-dBi gain in Figure 3(c). In other words, the six-element array in Figure 4 behaves as a retro-reflective beamformer; it generates a focal point in the near-zone, but its far-zone radiation is not as collimated as a retro-directive beamformer's. According to our numerical simulations, retro-reflective beamforming

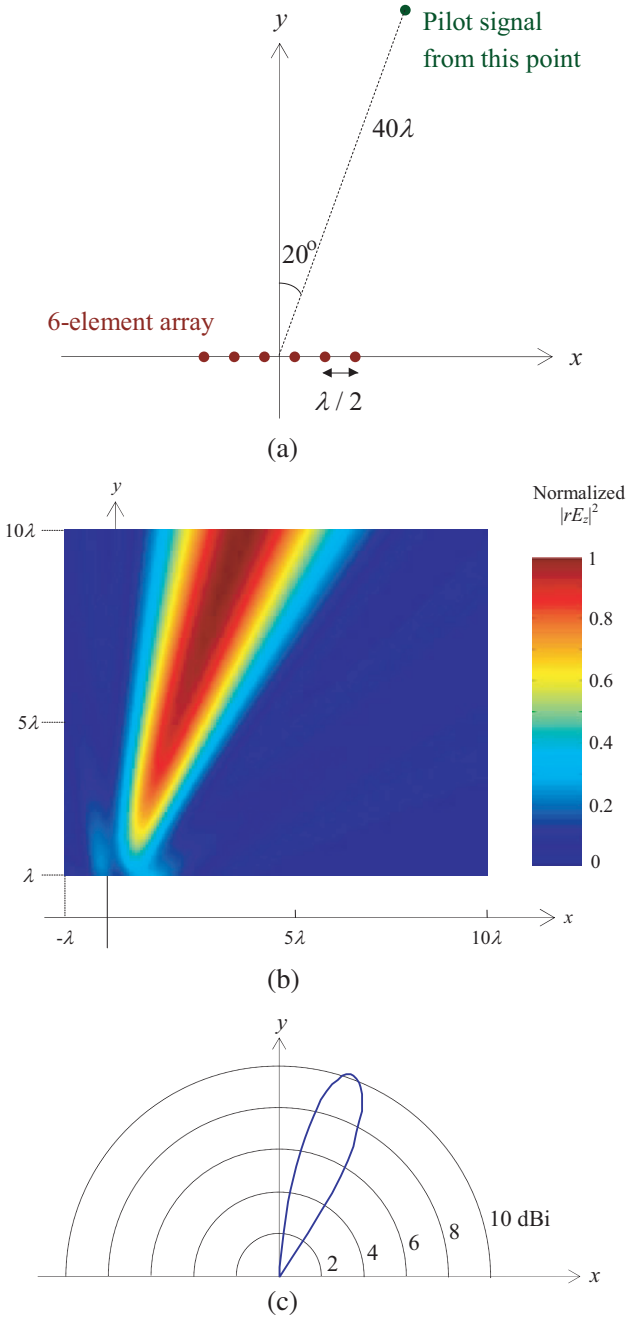

Figure 3. Simulation results of equi-spaced array with pilot signal from 40λ away. (a) Geometrical configuration (not to scale). (b) Distribution of electric field radiated from the array. (c) Far-zone gain radiated from the array.

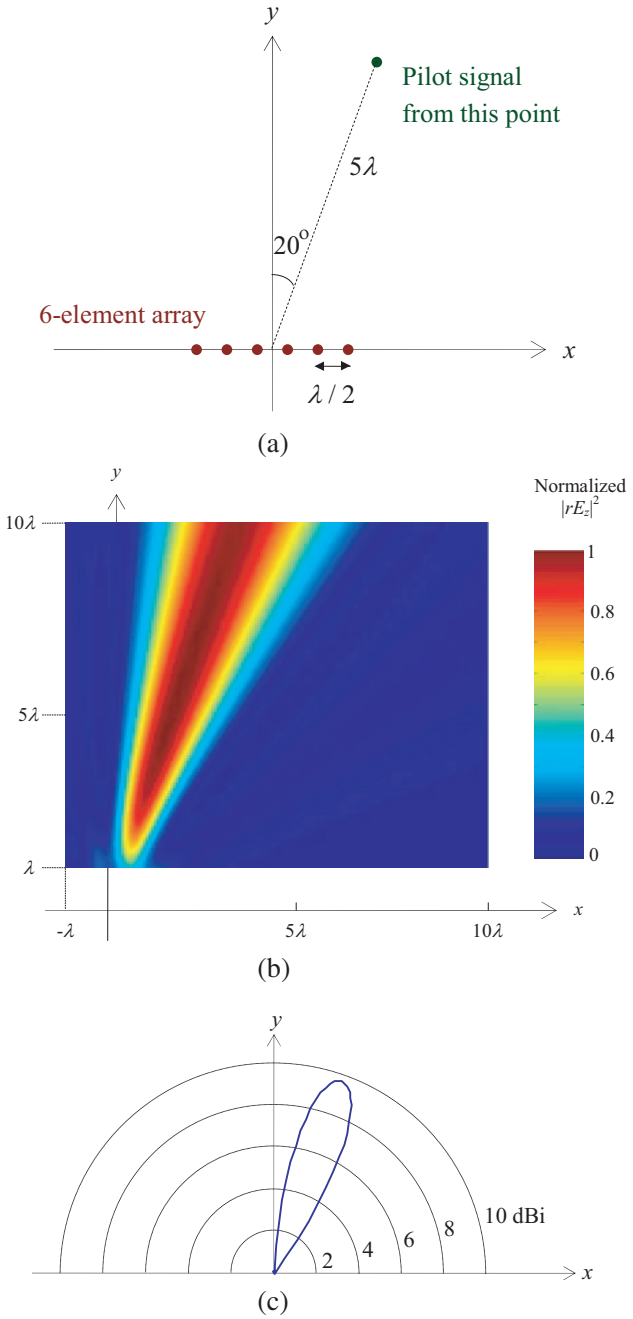

Figure 4. Simulation results of equi-spaced array with pilot signal from 5λ away. (a) Geometrical configuration. (b) Distribution of electric field radiated from the array. (c) Far-zone gain radiated from the array.

becomes more different from retro-directive beamforming in term of far-zone performance when the wireless power receiver moves closer to the wireless power transmitter and/or when the number of array elements in the wireless power transmitter increases.

The numerical examples in Figure 3 and Figure 4 reveal that a retro-directive beamformer behaves as a conventional phased array antenna whereas a retro-reflective beamformer behaves as a near-field

focusing antenna. To be more specific, a retro-reflective beamformer constructs a focal point in its near-zone and its maximum far-zone gain is lower than its retro-directive counterpart. In applications where mobile/portable electronic devices (such as wireless sensors) need to be charged wirelessly, the wireless power transmitter is not desired to construct any focal points other than the mobile/portable devices' location and its far-zone gain must be minimized to prevent electromagnetic interference. We therefore investigate further reducing the far-zone gain associated with retro-reflective beamforming through adjusting the array's geometrical configuration. Two types of array configurations other than linear equi-spaced array are investigated below.

The V-shaped array configuration illustrated in Figure 5(a) is obtained by deforming the linear equi-spaced array in Figure 4(a) to a "V" shape. All the other conditions remain unchanged between Figure 5(a) and Figure 4(a). The electric field radiated by the V-shaped array in response to a pilot signal from 5λ away is plotted in Figure 5(b). It is observed that the V-shape array generates a focal point at the location from which the pilot signal is broadcasted, as the equi-spaced array does. It is worth noting that in Figure 4(b) and Figure 5(b) $|rE_z|^2$ is normalized by the respective peak value, and the peak value of $|rE_z|^2$ in Figure 5(b) is almost the same as that in Figure 4(b) (to be exact, their relative difference is as small as 1.7%). Meanwhile, comparison between Figure 4(b) and Figure 5(b) clearly demonstrates that at locations far away from the spatial origin along $\phi = 70^\circ$ direction the electric field is more divergent in Figure 5(b) than in Figure 4(b). The V-shaped array generates a far-zone beam along $\phi = 70^\circ$ direction (as displayed in Figure 5(c)) with gain value of 9.2 dBi; it is 0.4 dB lower than the maximum gain value of Figure 4(c). Whereas Figure 4(c) exhibits no side lobes, side lobe appears in Figure 5(c), which is reasonable with the drop of main lobe's gain. In conclusion, deforming an equi-spaced array to V-shape reduces the maximum far-zone gain without affecting the near-zone focusing performance.

The configuration illustrated in Figure 6(a) is termed a "perturbed array:" on the basis of the linear equi-spaced array in Figure 4(a), and all the elements' spatial locations are perturbed randomly. Specifically,

$$\begin{cases} x_n = x_n^{(e)} + (\Delta x)_n = x_n^{(e)} + \alpha_n \times 0.1\lambda \\ y_n = y_n^{(e)} + (\Delta y)_n = y_n^{(e)} + \beta_n \times 0.1\lambda \\ z_n = z_n^{(e)} + (\Delta z)_n = z_n^{(e)} + \gamma_n \times 0.1\lambda \end{cases}, \quad n = 1, 2, \ldots, 6, \tag{1}$$

where (x_n, y_n, z_n), $n = 1, 2, \ldots, 6$, denote coordinates of the six elements in the perturbed array; $(x_n^{(e)}, y_n^{(e)}, z_n^{(e)})$, $n = 1, 2, \ldots, 6$, are the coordinates of the six elements in the equi-spaced array in Figure 4(a); $(\alpha_n, \beta_n, \gamma_n)$ are all random numbers uniformly distributed between -1 and 1. The perturbed array has similar characteristics to the V-shaped array: it reduces the maximum far-zone gain without affecting the near-zone focusing performance, as shown in Figure 6(b) and Figure 6(c). The gain value along $\phi = 70^\circ$ in Figure 6(c) is 8.7 dBi, 0.9 dB lower than the maximum gain value in Figure 4(c).

When the wireless power receiver resides 40λ distance away along $\phi = 70^\circ$ from the spatial origin, the three array configurations above (i.e., equi-spaced array, V-shaped array, and perturbed array) have little difference from one another in term of maximum far-zone gain value. It can be explained by the fundamental antenna theory. The radiation from any antenna configuration behaves plane waves in its far-zone [24]. As a result, interaction between the wireless power receiver and wireless power transmitter can be characterized by one explicit direction and retro-reflective beamforming reverts to retro-directive beamforming.

3. EXPERIMENTAL STUDIES OF RETRO-DIRECTIVE BEAMFORMING AND RETRO-REFLECTIVE BEAMFORMING

This section presents some of our experimental results to verify the numerical studies of Section 2. It is noted that there are some differences between the experimental setup in this section and the numerical setup in Section 2. For instance, in our experiments microstrip antennas and monopole antennas are employed, whereas in our numerical simulations Hertzian dipoles are used for antennas. This difference is largely because we have difficulty to incorporate the precise models of microstrip antennas or monopole antennas into the simulations of Section 2. Since this paper focuses on beamforming performance, which

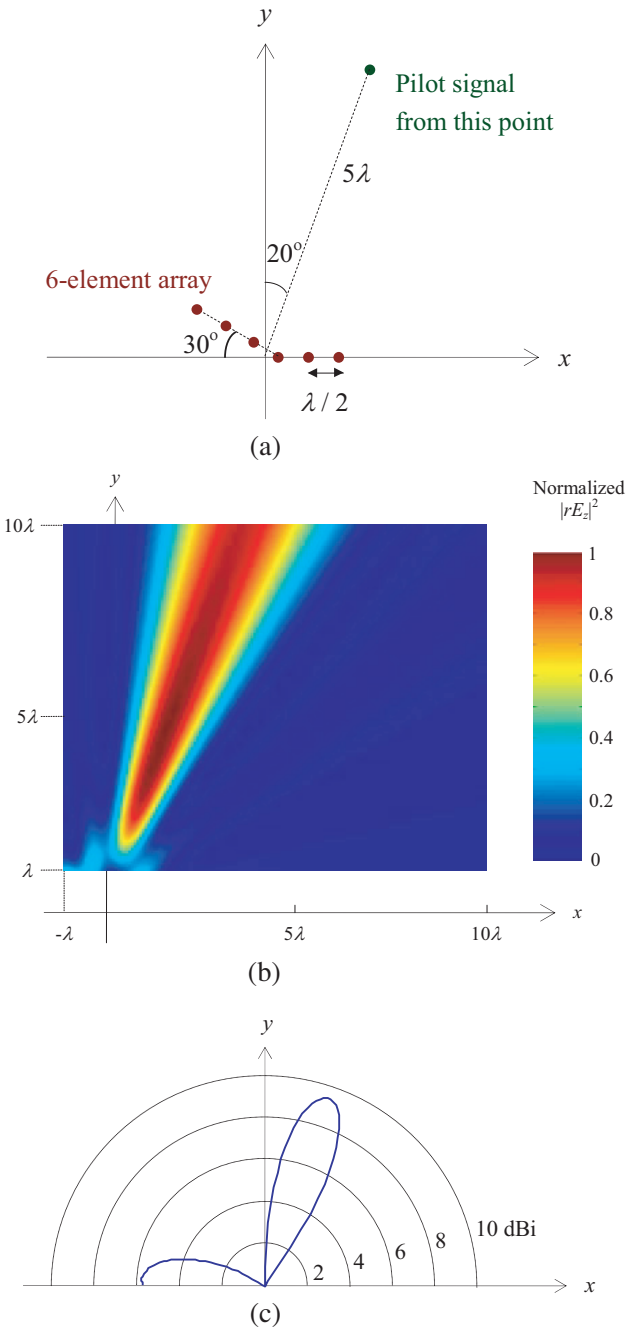

Figure 5. Simulation results of V-shaped array with pilot signal from 5λ away. (a) Geometrical configuration. (b) Distribution of electric field radiated from the array. (c) Far-zone gain radiated from the array.

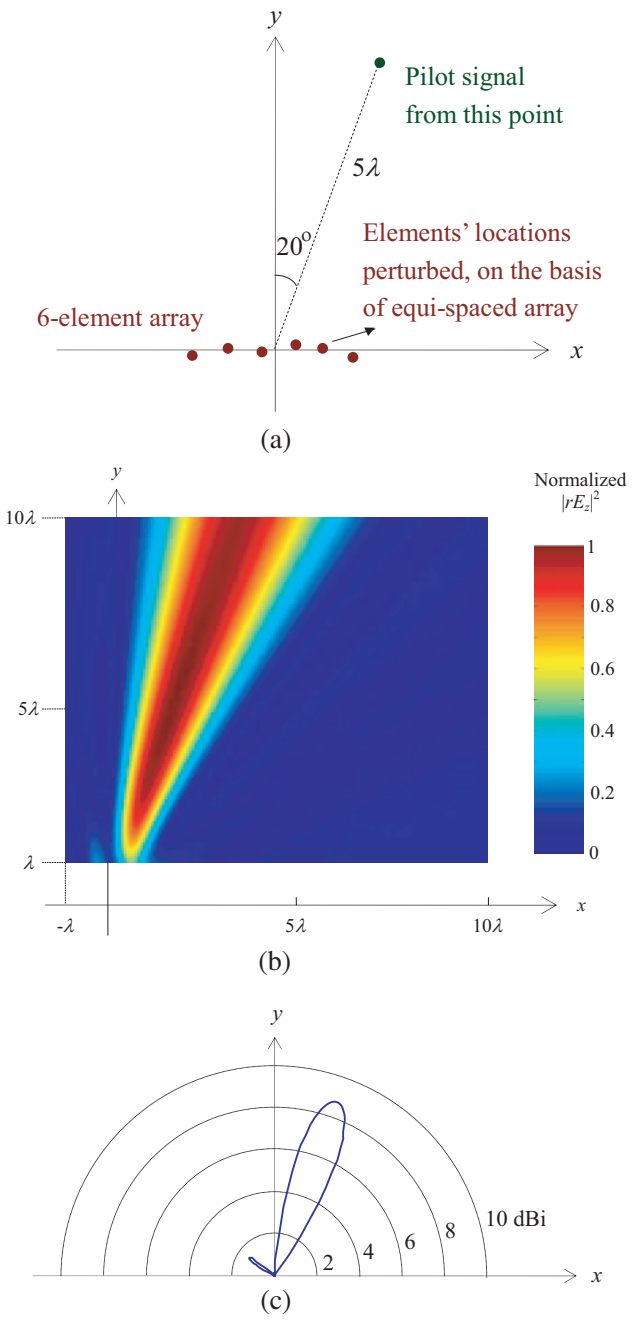

Figure 6. Simulation results of perturbed array with pilot signal from 5λ away. (a) Geometrical configuration. (b) Distribution of electric field radiated from the array. (c) Far-zone gain radiated from the array.

is primarily determined by array factor, the choice of individual antenna elements (such as microstrip, monopole, or Hertzian dipole) does not impact the major conclusions of this paper.

In all of our experiments, the wireless power receiver includes a monopole antenna made of copper wire with length 34.5 mm, and the wireless power transmitter consists of six microstrip antenna elements. The six microstrip antenna elements are identical to each other. They are deployed into three array

configurations and studied separately: equi-spaced array, V-shaped array, and perturbed array. One of our experimental setups is shown in Figure 7, in which the six antenna elements are configured into a linear equi-spaced array. Each rectangular microstrip patch has dimensions 31.4 mm along z direction and 46 mm along x direction. The microstrip antennas and monopole antenna are all linearly polarized along z direction. An individual microstrip patch antenna generates a main radiation beam toward $+y$ direction with gain value of 4 dBi at 2.12 GHz. The monopole antenna has omni-directional radiation pattern in the x-y plane with gain value of 0.1 dBi at 2.12 GHz (the monopole antenna in our experiments is not optimized; however, its low gain has no impact on characterizing the retro-directive or retro-reflective arrays).

All of our experiments are conducted at frequency $f = 2.12$ GHz. Every experiment consists of two steps. In the first step, a continuous-wave pilot signal at frequency f is broadcasted by the monopole antenna, and the pilot signal is received by the six microstrip antennas. The pilot signal's phases received by the six microstrip antennas in the first step are denoted as $-\theta_1, -\theta_2, \ldots, -\theta_6$. In the second step, wireless power in the form of continuous-wave at frequency f is radiated by the six microstrip antennas. The six microstrip antennas are excited with uniform amplitude in the second step. The power radiated by each microstrip antenna is 21 dBm = 125 mW, and the total transmitted power $P_t = 125\,\text{mW} \times 6 = 750\,\text{mW}$. In the second step, the six microstrip antennas are excited with phases $\theta_1, \theta_2, \ldots, \theta_6$, respectively. The monopole antenna moves over a certain region in the x-y plane to detect wireless power; the power level is read by a power meter directly connected to the monopole antenna. All the circuits are implemented using commercial off-the-shelf components or commercially-available equipment, as described in [21].

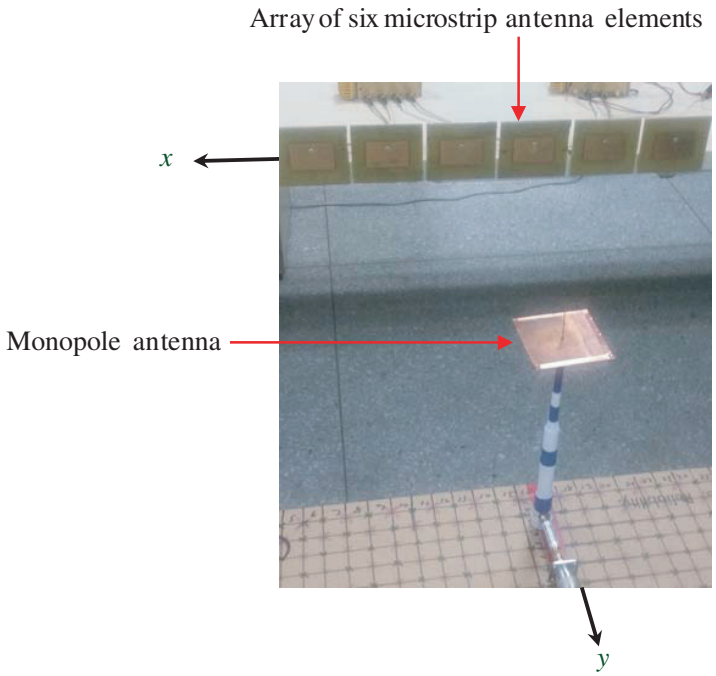

Figure 7. A photo of experimental setup.

Geometrical configuration and experimental results related to the equi-spaced array are depicted in Figure 8. The pilot signal is broadcasted from ($x = 0.8$ m, $y = 4$ m) in the first step. In the second step, power received by the monopole antenna, P_r, is measured to be -11.51 dBm when the monopole antenna is located at ($x = 0.8$ m, $y = 4$ m). By making use of Friis transmission equation [24]

$$\frac{P_r}{P_t} = \frac{\lambda^2 G_t G_r}{(4\pi d)^2}, \tag{2}$$

gain value of the six-element array, G_t, is calculated as

$$G_t = \frac{P_r}{P_t}\frac{(4\pi d)^2}{\lambda^2 G_r} = 10.82\,\text{dBi}, \tag{3}$$

where $\lambda = c/f$ is the wavelength, $G_r = 0.1\,\text{dBi}$ the gain of monopole antenna, and distance $d = \sqrt{4^2 + 0.8^2}\,\text{m}$. In Figure 8(b), the values of G_t calculated based on measurement data are plotted. G_t, rather than the received power, is plotted in order to visualize the far-zone behavior more clearly. In fact, Figure 8 corresponds to the numerical example in Figure 3, and in Figure 3 $|rE_z|^2$ (rather than $|E_z|^2$) is plotted due to the same concern. Obviously, the peak values of G_t are located at ($x = 0.2\,\text{m}$, $y = 1\,\text{m}$), ($x = 0.4\,\text{m}$, $y = 2\,\text{m}$), ($x = 0.6\,\text{m}$, $y = 3\,\text{m}$), and ($x = 0.8\,\text{m}$, $y = 4\,\text{m}$). Because Friis transmission equation is valid in the far-zone only, G_t associated with small y values does not accurately reflect the far-zone gain. However with the increase of y, the peak G_t converges to 10.8 dBi, indicating a far-zone gain of 10.8 dBi toward the incoming direction of pilot signal.

Figure 9(a) has only one difference compared to Figure 8(a): the pilot signal is broadcasted from ($x = 0.2\,\text{m}$, $y = 1\,\text{m}$) in the first step. Comparison between Figure 8(b) and Figure 9(b) reveals that Figure 9(b) has higher power level at ($x = 0.2\,\text{m}$, $y = 1\,\text{m}$) than Figure 8(b) (to be specific, 1.5 dB higher), and Figure 8(b) has higher power level at ($x = 0.8\,\text{m}$, $y = 4\,\text{m}$) than Figure 9(b) (to be specific, 1 dB higher). It is as expected, since wireless power is focused onto the location from which pilot signal is broadcasted. In Figure 9, the six-element array behaves as a retro-reflective beamforer: a focal point is generated in the array's near-zone, and its maximum far-zone gain is 1 dB lower than the maximum far-zone gain of the retro-directive beamformer in Figure 8.

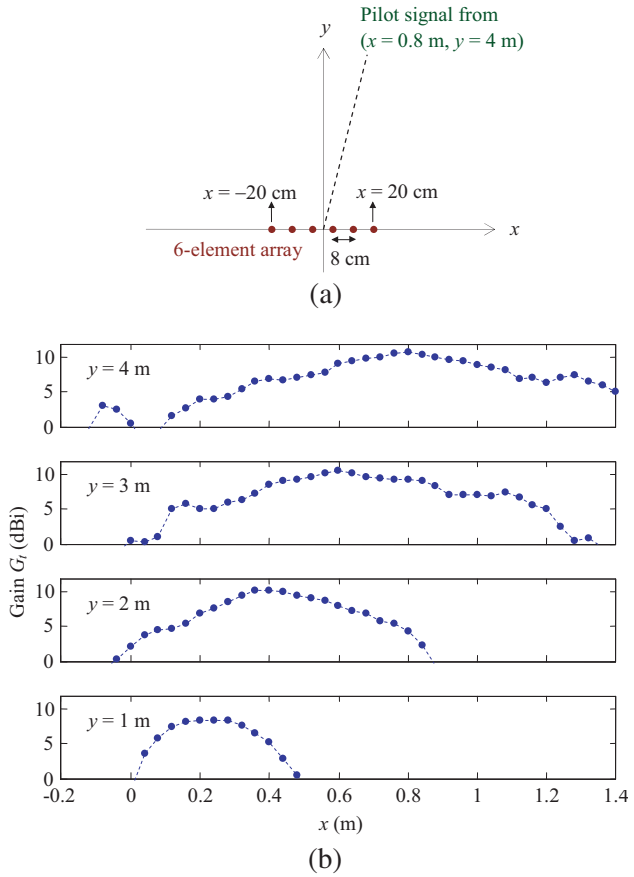

Figure 8. Measurement results of equi-spaced array with pilot signal from ($x = 0.8\,\text{m}$, $y = 4\,\text{m}$). (a) Geometrical configuration (not to scale). (b) Gain G_t calculated based on measurement data.

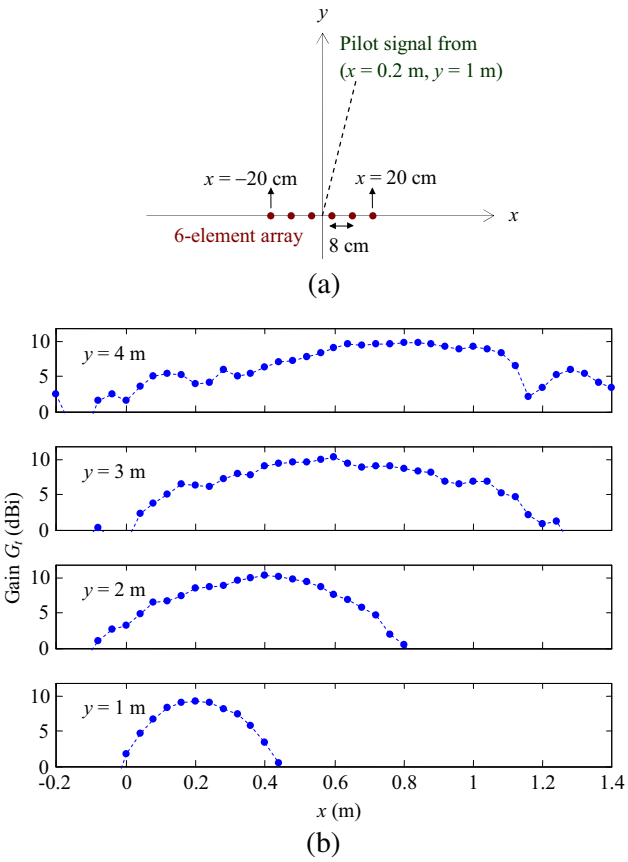

Figure 9. Measurement results of equi-spaced array with pilot signal from ($x = 0.2\,\text{m}$, $y = 1\,\text{m}$). (a) Geometrical configuration (not to scale). (b) Gain G_t calculated based on measurement data.

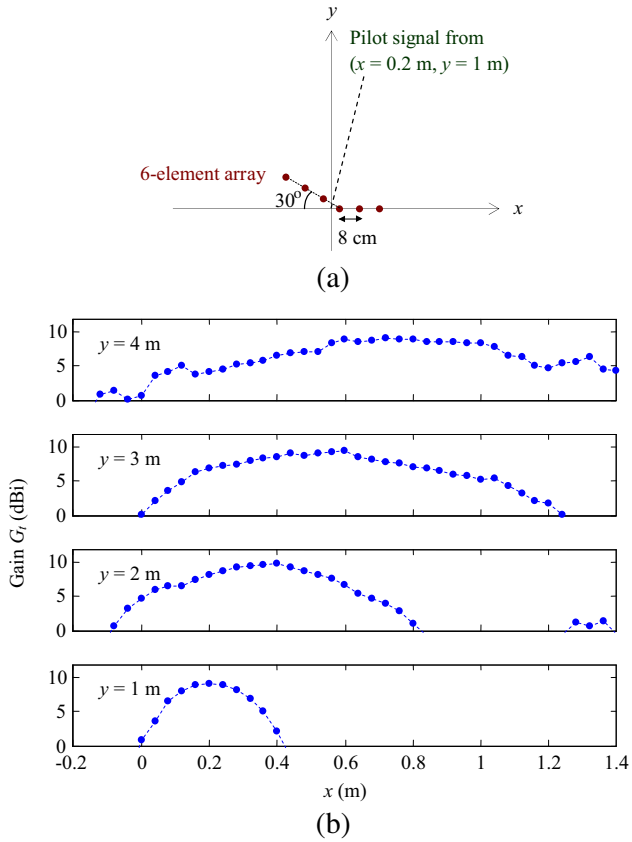

Figure 10. Measurement results of V-shaped array with pilot signal from ($x = 0.2\,\text{m}$, $y = 1\,\text{m}$). (a) Geometrical configuration (not to scale). (b) Gain G_t calculated based on measurement data.

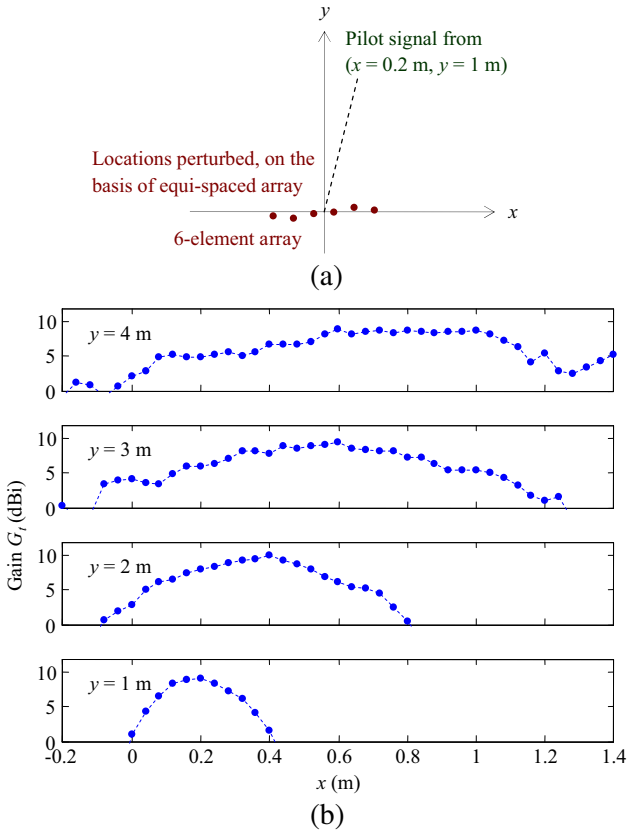

Figure 11. Measurement results of perturbed array with pilot signal from ($x = 0.2\,\text{m}$, $y = 1\,\text{m}$). (a) Geometrical configuration (not to scale). (b) Gain G_t calculated based on measurement data.

Figure 10 corresponds to the numerical example in Figure 5. As illustrated in Figure 10(a), the six microstrip antenna elements are configured into a V-shaped array. All the other conditions remain unchanged between Figure 9(a) and Figure 10(a). It is observed from Figure 10(b) that the V-shaped array generates a focal point at ($x = 0.2\,\text{m}$, $y = 1\,\text{m}$), the location from which the pilot signal is broadcasted. Meanwhile, it is observed that the power level at ($x = 0.2\,\text{m}$, $y = 1\,\text{m}$) in Figure 10(b) is almost the same as that in Figure 9(b). It means that deforming the equi-spaced array to V-shape does not impact the array's performance in term of near-zone focusing. However, Figure 9 and Figure 10 demonstrate different far-zone performances. Specifically, the far-zone gain at ($x = 0.8\,\text{m}$, $y = 4\,\text{m}$) in Figure 10 is 1 dB lower than that in Figure 9. Therefore, the experimental data in Figure 10 verify the conclusions drawn from Figure 5: it is possible to reduce the maximum far-zone gain of retro-reflective beamforming by adjusting the array's geometrical configuration without affecting the near-zone focusing performance.

Figure 11 studies the perturbed array, and it corresponds to the numerical example in Figure 6. The geometrical configuration in Figure 11(a) is obtained by perturbing the locations of the six antenna elements in Figure 9(a). In the numerical example of Figure 6, the locations are perturbed along all the three directions (that is, x, y, and z); nevertheless in our experiments, perturbation is applied along y and z directions, but not along x direction. As shown in Figure 7, the six microstrip antennas almost touch each other along x direction in the equi-spaced array, and as a result, perturbation along x direction could create strong undesired mutual coupling among the six antennas. Therefore on the basis of the equi-spaced array, the six antenna elements' locations are perturbed along y and z directions only in our experiments. The specific perturbation data are listed below.

Element 1: $(\Delta y)_1 = -13\,\text{mm} \quad (\Delta z)_1 = 0$
Element 2: $(\Delta y)_2 = -20\,\text{mm} \quad (\Delta z)_2 = -5\,\text{mm}$
Element 3: $(\Delta y)_3 = -6\,\text{mm} \quad (\Delta z)_3 = 3\,\text{mm}$
Element 4: $(\Delta y)_4 = 0 \quad (\Delta z)_4 = 0$
Element 5: $(\Delta y)_5 = 14\,\text{mm} \quad (\Delta z)_5 = -3\,\text{mm}$
Element 6: $(\Delta y)_6 = 7\,\text{mm} \quad (\Delta z)_6 = 2\,\text{mm}$

Although perturbation is not conducted along all the three directions, the results in Figure 11 verify the conclusions drawn from Figure 6. The power level at the focal point, ($x = 0.2\,\text{m}$, $y = 1\,\text{m}$), in Figure 11 is the same as those in Figure 9 and Figure 10. Meanwhile, the far-zone gain at ($x = 0.8\,\text{m}$, $y = 4\,\text{m}$) in Figure 11 is about 1 dB lower than that in Figure 9. It is therefore concluded that perturbation of array elements' locations reduces the maximum far-zone gain of retro-reflective beamforming without affecting the near-zone focusing performance.

In Table 1, the four cases investigated in this section are compared with one another in term of maximum far-zone gain value. In Case (i), the six-element equi-spaced array behaves as a retro-directive beamformer; it generates a gain value as large as 10.82 dBi. In Case (ii), the equi-spaced array is a retro-reflective beamformer; its maximum far-zone gain drops to 9.88 dBi. Deforming the equi-spaced array to V-shape or perturbed configuration results in further lower far-zone gain values, roughly 9 dBi to be specific.

Table 1. Comparison among the four cases in Section 3.

Case	Configuration	Maximum far-zone gain
(i)	Equi-spaced array, with pilot signal from ($x = 0.8\,\text{m}$, $y = 4\,\text{m}$)	10.82 dBi
(ii)	Equi-spaced array, with pilot signal from ($x = 0.2\,\text{m}$, $y = 1\,\text{m}$)	9.88 dBi
(iii)	V-shaped array, with pilot signal from ($x = 0.2\,\text{m}$, $y = 1\,\text{m}$)	9 dBi
(iv)	Perturbed array, with pilot signal from ($x = 0.2\,\text{m}$, $y = 1\,\text{m}$)	8.96 dBi

4. CONCLUSIONS

In this paper, theoretical and experimental studies are conducted on the difference between retro-directive beamforming and retro-reflective beamforming in the context of wireless power transmission applications. In all of our studies, a wireless power receiver broadcasts continuous-wave pilot signal; the wireless power transmitter receives and analyzes the pilot signal; finally, the wireless power transmitter transmits continuous-wave power with phase profile conjugate to the pilot signals' phase profile. Three primary conclusions are drawn from our studies. First, when the wireless power receiver resides in the far-zone of wireless power transmitter, retro-directive beamforming and retro-reflective beamforming are identical to each other. Second, when the wireless power receiver is not in the far-zone of wireless power transmitter, retro-reflective beamforming is capable of focusing power onto the wireless power receiver's location, but retro-directive beamforming is not applicable. Third, it is possible to reduce retro-reflective beamforming's maximum far-zone gain via adjusting the geometrical configurations without affecting its near-zone focusing performance. We find it particularly interesting to compare an equi-spaced retro-reflective array and a "perturbed retro-reflective array" (which is obtained by perturbing the locations of the equi-spaced array's antenna elements). The results in this paper suggest that perturbation is a simple and effective method to reduce retro-reflective beamforming's far-zone gain. We are currently conducting more in-depth research on this topic.

ACKNOWLEDGMENT

This work was supported in part by the National Natural Science Foundation of China Grant 61471195, National Natural Science Foundation of China Grant 61102032, National Science Foundation Grant ECCS 1303142, and National Science Foundation Grant ECCS 1503600.

REFERENCES

1. Strassner, B. and K. Chang, "Microwave power transmission: Historical milestones and system components," *Proceedings of the IEEE*, Vol. 101, No. 6, 1379–1396, June 2013.
2. Visser, H. J. and R. J. M. Vullers, "RF energy harvesting and transport for wireless sensor network applications: Principles and requirements," *Proceedings of the IEEE*, Vol. 101, No. 6, 1410–1423, June 2013.
3. Zhai, H., H. K. Pan, and M. Lu, "A practical wireless charging system based on ultra-wideband retro-reflective beamforming," *IEEE International Antennas and Propagation Symposium*, Toronto, Canada, July 2010.
4. Mazurenko, O. and Y. Yakornov, "Focused arrays beamforming," *Behaviour of Electromagnetic Waves in Different Media and Structures*, 419–440, A. Akdagli, Ed., InTech, Rijeka, 2011.
5. Kildal, P.-S. and M. M. Davis, "Characterization of near-field focusing with application to low altitude beam focusing of the Arecibo tri-reflector system," *IEE Proceedings — Microwaves Antennas and Propagation*, Vol. 143, No. 4, 284–292, August 1996.
6. Reid, D. R. and G. S. Smith, "A comparison of the focusing properties of a Fresnel zone plate with a doubly-hyperbolic lens for application in a free-space, focused beam measurement system," *IEEE Transactions on Antennas and Propagation*, Vol. 57, No. 2, 499–507, February 2009.
7. Chou, H.-T., T.-M. Hung, N.-N. Wang, H.-H. Chou, C. Tung, and P. Nepa, "Design of a near-field focused reflectarray antenna for 2.4 GHz RFID reader applications," *IEEE Transactions on Antennas and Propagation*, Vol. 59, No. 3, 1013–1018, March 2011.
8. Karimkashi, S. and A. A. Kishk, "Focusing properties of Fresnel zone plate lens antennas in the near-field region," *IEEE Transactions on Antennas and Propagation*, Vol. 59, No. 5, 1481–1487, May 2011.
9. Gomez-Tornero, J. L., D. Blanco, E. Rajo-Iglesias, and N. Llombart, "Holographic surface leaky-wave lenses with circularly-polarized focused near-fields — Part I: Concept, design and analysis theory," *IEEE Transactions on Antennas and Propagation*, Vol. 61, No. 7, 3475–3485, July 2013.
10. Monnai, Y. and H. Shinoda, "Focus-scanning leaky-wave antenna with electronically pattern-tunable scatterers," *IEEE Transactions on Antennas and Propagation*, Vol. 59, No. 6, 2070–2077, June 2011.
11. Okuyama, T., Y. Monnai, and H. Shinoda, "20-GHz focusing antennas based on corrugated waveguide scattering," *IEEE Antennas and Wireless Propagation Letters*, Vol. 12, 1284–1286, 2013.
12. Buffi, A., P. Nepa, and G. Manara, "Design criteria for near-field-focused planar arrays," *IEEE Antennas and Propagation Magazine*, Vol. 54, 40–50, 2012.
13. Tuan, S.-C. and H.-T. Chou, "Analytic analysis of transient radiation from phased array antennas in the near- and far-field focus applications," *IEEE Transactions on Antennas and Propagation*, Vol. 61, No. 5, 2519–2531, May 2013.
14. Leon, G. and F. Las-Heras, "Fresnel-zone-based focused planar array," *IEEE Antennas and Wireless Propagation Letters*, Vol. 13, 165–168, 2014.
15. Stephan, K. D., J. B. Mead, D. M. Pozar, L. Wang, and J. A. Pearce, "A near field focused microstrip array for a radiometric temperature sensor," *IEEE Transactions on Antennas and Propagation*, Vol. 55, No. 4, 1199–1203, April 2007.
16. Bogosanovic, M. and A. G. Williamson, "Microstrip antenna array with a beam focused in the near-field zone for application in noncontact microwave industrial inspection," *IEEE Transactions on Instrumentation and Measurement*, Vol. 56, No. 6, 2186–2195, December 2007.
17. Buffi, A., A. A. Serra, P. Nepa, H.-T. Chou, and G. Manara, "A focused planar microstrip array for 2.4 GHz RFID readers," *IEEE Transactions on Antennas and Propagation*, Vol. 58, No. 5, 1536–1544, May 2010.
18. Karimkashi, S. and A. A. Kishk, "Focused microstrip array antenna using a Dolph-Chebyshev near-field design," *IEEE Transactions on Antennas and Propagation*, Vol. 57, No. 12, 3813–3820, December 2009.

19. Alvarez, J., R. G. Ayestaran, G. Leon, L. F. Herran, A. Arboleya, J. A. Lopez-Fernandez, and F. Las-Heras, "Near field multifocusing on antenna arrays via non-convex optimisation," *IET Microwaves, Antennas & Propagation*, Vol. 8, No. 10, 754–764, July 2014.
20. Siragusa, R., P. Lemaitre-Auger, and S. Tedjini, "Tunable near-field focused circular phase-array antenna for 5.8-GHz RFID applications," *IEEE Antennas and Wireless Propagation Letters*, Vol. 10, 33–36, 2011.
21. Wang, X., S. Sha, J. He, L. Guo, and M. Lu, "Wireless power delivery to low-power mobile devices based on retro-reflective beamforming," *IEEE Antennas and Wireless Propagation Letters*, Vol. 13, 919–922, 2014.
22. He, J., X. Wang, L. Guo, S. Shen, and M. Lu, "A distributed retro-reflective beamformer for wireless power transmission," *Microwave and Optical Technology Letters*, Vol. 57, No. 8, 1873–1876, August 2015.
23. Wang, X., X. Hou, L. Wang, and M. Lu, "Employing phase-conjugation antenna array to beam microwave power from satellite to earth," *IEEE International Conference on Wireless for Space and Extreme Environments*, Orlando, FL, December 2015.
24. Balanis, C. A., *Antenna Theory: Analysis and Design*, 3rd Edition, Wiley-Interscience, 2005.